PROCEEDINGS OF SCIENCE

Seasonal variation of the atmospheric muon flux in the KM3NeT detectors

J. M. Mulder[a,*] and R. Bruijn[a,b] for the KM3NeT Collaboration

[a] *University of Amsterdam, Institute of Physics/IHEF, PO Box 94216,Amsterdam, 1090 GE Netherlands*

[b] *Nikhef, National Institute for Subatomic Physics, PO Box 41882, Amsterdam, 1009 DB Netherlands*

E-mail: J.Mulder@nikhef.nl, rbruijn@nikhef.nl, km3net-pc@km3net.de

KM3NeT is constructing two large volume water Cherenkov detectors in the Mediterranean Sea. By instrumenting the water with photo-multipliers, neutrinos can be detected through the Cherenkov light from charged products of their interactions. The dominating signal, however, comes from muons created in extensive air-showers resulting from cosmic ray interactions in the top of the atmosphere. Despite the water column above, the highest-energy muons (> TeV) reach the detectors. Air-showers develop in a non-isotropic atmosphere where the vertical temperature profile, and thus the density, varies over time. The changing density of the atmosphere affects the balance between interaction and decay (to muons) of mesons in the air-showers. Therefore, the muon flux is expected to correlate with the seasons and short-term temperature fluctuations, as confirmed by other experiments. In this contribution, we present a first measurement of the correlation of the detected muon rate with the effective atmospheric temperature (weighted by muon production spectrum and detector response) for the KM3NeT ORCA telescope. The measured rate is compared with simulations, which model the time-dependent detector efficiency and environmental factors for a constant atmospheric muon flux.

38th International Cosmic Ray Conference (ICRC2023)
26 July - 3 August, 2023
Nagoya, Japan

*Speaker

PoS(ICRC2023)355

1. Introduction

Extensive air-showers initiated by interactions of cosmic rays develop in the atmosphere. After the initial interaction, many particles are created through re-interaction of the products with molecules in the air, and through decays of unstable particles. Muons and neutrinos are created through such decays, mostly from the light mesons: pions and kaons. In regions where the density is higher such particles have a higher probability to interact. When the density is lower, the balance shifts towards decaying before re-interaction. As the atmosphere is dynamic, in the sense that the vertical temperature and thus density profile changes with time and location, the amount of muons and neutrinos created varies with time. This seasonal variation of the muon and neutrino flux is well measured by a multitude of underground detectors such as [1, 2, 5, 6, 8–10, 17, 19].

KM3NeT consists of two large-volume water-Cherenkov detectors, designed to detect neutrino interactions. The smaller (7Mt when completed) ORCA detector, anchored at 2450 meters of depth near Toulon, France, focuses on the determination of the neutrino mass ordering and oscillation parameters. The larger (1 Gt when completed) ARCA detector, anchored at 3500 meters of depth near Capo Passero, Italy, focuses on cosmic neutrino detection. Both detectors share the same technology. Pressure resistant glass spheres with a diameter of about 17 inches, house 31 light-sensitive 3-inch photo-multiplier tubes (PMTs) together with electronics for control, nanosecond timing and readout. These so-called optical modules are organised in vertical structures called detection units. These consist of two dyneema ropes along the whole length, to which 18 (buoyant) modules are connected, a backbone cable with power cables and optical fibres going to each module, and an anchor housing an electronics container. Power is provided from shore through a sea-floor network, which also houses an optical-fibre network for data transport. Both detectors are currently being expanded. Intermediate configurations of the detectors are referred to either ORCA-X or ARCA-X, where X is the amount of detection units operational.

The aforementioned studies have used variations of the same equations that describe the relation between the atmospheric temperature and muon rate. In line with that, we start here from the relation[9, 11, 15]

$$\frac{\Delta R}{\langle R \rangle} = \alpha_T \frac{\Delta T_{eff}}{\langle T_{eff} \rangle} \tag{1}$$

where ΔR is the deviation of the muon rate with respect to the average muon rate $\langle R \rangle$, and ΔT_{eff} the deviation of the *effective temperature* from the average effective temperature $\langle T_{eff} \rangle$. This relation is a simplified form, where the atmosphere is approximated as isothermal with temperature T_{eff}. The effective temperature takes into account that the muon production spectrum P_μ is dependent on the depth in the atmosphere χ[1], while the temperature also depends on the depth. The correlation coefficient, depends on the muon energies to which a detector is sensitive, through the details of the muon production, in particular the ratio of pions and kaons in the relevant energy range. In our definition of T_{eff} the energy and zenith angle θ dependent response of the detector is taken into account via the effective area A_{eff}. The effective temperature is in essence the depth dependent temperature profile, weighted with the energy and zenith dependent muon production spectrum and

[1]This is the column density as integrated from the top of the atmosphere.

detector response

$$T_{eff} = \frac{\int d\chi T(\chi) \left[\int dE_0 \int d\theta P_\mu(E_0,\theta,\chi) A_{eff}(E_0,\theta)\right]}{\int d\chi \left[\int dE_0 \int d\theta P_\mu(E_0,\theta,\chi) A_{eff}(E_0,\theta)\right]} \tag{2}$$

where E_0 is the muon energy at sea-level. For this first study in the context of KM3NeT, an analytical model based on cascade-equations from [14] is used for the muon production spectrum P_μ. In this contribution, we present a new method to measure the atmospheric muon rate in the KM3NeT detectors. This method accounts for the fluctuations in the muon rate which are not due to changes in the atmosphere, but due to environmental conditions and detector effects.

2. Dynamic environment and detector

A particular challenge in measuring the variation of the muon rate in the KM3NeT detectors results from the fact that the detectors operate in a uncontrolled, dynamic environment. The photo-detection rate of the photo-multiplier tubes is dominated by light from ^{40}K decays and bioluminescence. While the rate from ^{40}K decay is rather constant, the bioluminescence is highly dynamic both in time and intensity. The baseline counting rate per KM3NeT PMT is about 7 kHz, with excursions of almost a factor 10 higher [3, 4]. Long term studies on median PMT counting rates in ANTARES [13] indicate fluctuations at various timescales including monthly and yearly. Such variations influence the muon detection rate. A moderately increased count-rate can increase the detection efficiency, while an instantaneous high count-rate may trigger a high-rate veto at the level of an optical module, suppressing the detection efficiency.

3. Simulation of muon flux and detector response

To simulate the muon flux at detector level, the fast parametric muon flux simulation software Mupage [12] is used. Single and multiple muon events are generated on a surface close to and surrounding the detector volume in the water. Efforts of re-tuning the parameters of Mupage on simulation and data are ongoing within KM3NeT, with the aim to improve the description and understanding of the atmospheric muon flux [18]. The tuning used in this analysis [16] is specific for the detector configuration. It represents a simulated flux constant in time, and thus not subject to atmospheric conditions. This is a key ingredient to this method.

The KM3NeT data taking happens in scheduled time periods of 6 hours which are called runs. The simulation scheme of KM3NeT makes use of the recorded PMT counting rates, which are stored for each PMT with a resolution of 100 µs for each run. In this so-called run-by-run simulation scheme, background photons are added to the photons resulting from the muons according to the recorded rates within a run. Also the time-dependent measured photon detection efficiencies of the PMTs are taken into account. In order to extract the effective area A_{eff}, Mupage simulations are used, re-weighted into a single-muon flux. As the effective area needs to be expressed in energy at sea-level, a depth and angle dependent energy loss correction is applied per muon.

4. Method

In order to extract the variations due to the changing muon flux, free from effects of the environment and detector response, a new method has been developed. The underlying presumption of the method is that the run-by-run simulation accounts for the influence of the ambient conditions and detector effects which are reflected in the PMT count-rates, *except* the variations caused by a change in muon flux. We define a time-dependent ratio of the recorded muon rate and the simulated muon rate:

$$R_{\frac{data}{sim}}(t) = \frac{R_{data}(t)}{R_{sim}(t)} \tag{3}$$

An average value of the of value $R_{\frac{data}{sim}}(t)$ is indicated by $\langle R_{\frac{data}{sim}} \rangle$. When the muon flux is properly described by the simulation, the average ratio should be 1. In case of the tuned Mupage muon flux parametrization for the ORCA-6 configuration and time period considered here, this is essentially the case with a value of $\langle R_{\frac{data}{sim}} \rangle = 1.015 \pm 0.0005$. We define a deviation in the muon rate ratio as

$$\Delta R_{\frac{data}{sim}}(t) = R_{\frac{data}{sim}}(t) - \langle R_{\frac{data}{sim}} \rangle \tag{4}$$

To study the variation of the muon rate variation with effective temperature, we define equivalently to eq. 1

$$\frac{\Delta R_{\frac{data}{sim}}}{\langle R_{\frac{data}{sim}} \rangle} = \alpha_{T,\frac{data}{sim}} \frac{\Delta T_{eff}}{\langle T_{eff} \rangle} \tag{5}$$

with the underlying presumption that $\alpha_{T,\frac{data}{sim}} = \alpha_T$ if all ambient and detector effects on the muon count rate are taken into account.

5. Data and simulation selection

The KM3NeT muon data analysed in this contribution is from the ORCA-6 detector and covers a period from `2020-01-26` to `2021-11-18`, with a total livetime of 374.59 days. Some data that was excluded in this analysis would be accepted with the latest quality criteria. Selections are applied to the data to remove events that are due to neutrinos, have badly reconstructed tracks in terms of angular resolution, or are caused by ambient light. The implementation of these selections include rejecting events that come from below (through the Earth); have a reconstructed energy below 8 GeV; or have a too low likelihood value. All events in this analysis fired at least the trigger aimed at identifying muon tracks. After selection, the median zenith and angular resolution on the muon direction, evaluated from simulation, are 0.422° and 0.708° respectively. The dataset consisted of 1.648×10^8 data events with $\langle R_{\text{data}} \rangle = 5.0884 \pm 0.0056$Hz and 1.623×10^8 simulations events with $\langle R_{\text{mc}} \rangle = 5.0127 \pm 0.0045$Hz.
The atmospheric temperature profile is downloaded from the public data repository of NASA's Atmospheric Infrared Sounder (AIRS) satellite [7]. The data covers the atmospheric column above the location of the ORCA detector between 42° − 43° latitude and 5° − 7° longitude in a 1-by-1 degree grid. The dataset provides temperature measurements at `01:30` and `13:30` (so twice a day), and on 24 different pressure levels, from 1 to 1000 hPa, together with error estimates. In figure 1(left), the atmospheric temperature profile for the whole period is shown. One can notice slow variation in spring and summer, but also shorter time-scale variations in the stratosphere such as

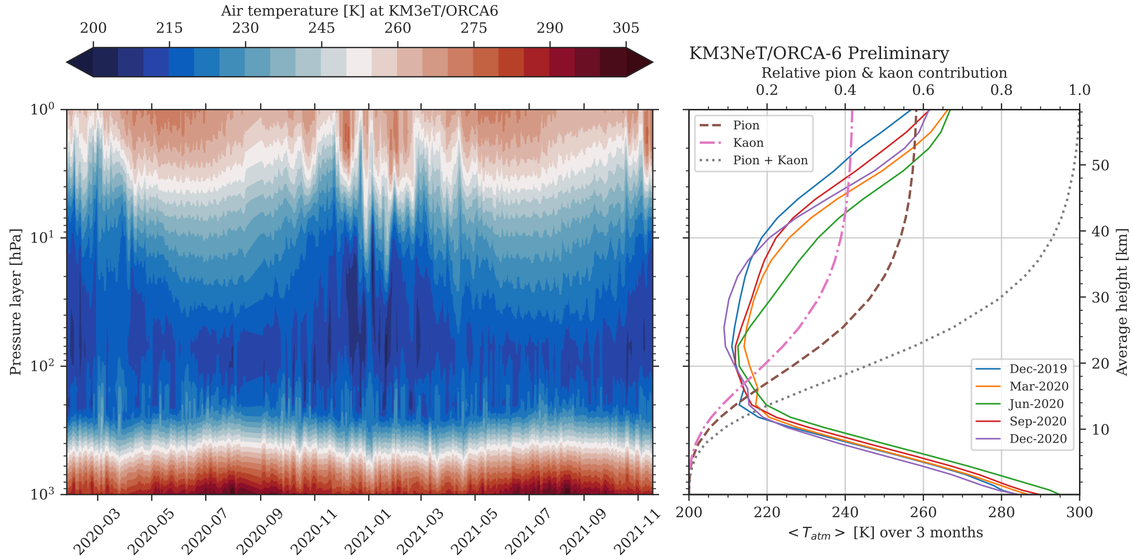

Figure 1: The atmospheric temperature above the ORCA detector in the period of ORCA-6 (left) and its 3-month average profiles (solid lines) for the year 2020. They share the left pressure axis which is given in 24 discrete layers[7]. The dashed lines (right) are the product of A_{eff} with the pion-only, kaon-only and combined muon production spectrum P_μ, integrated over energy and zenith angle. The shared right axis shows the average geometrical height that corresponds to the pressure.

those which are very prominent for all winter periods covered. In figure 1(right) these profiles are averaged over 3 month periods for 2020 and are labeled according to the starting month. Noticeable is the different profiles for the the first and last December (each holding roughly same number of measurements). The same figure also shows the depth dependent product of the effective area with the muon production profiles, separate for pions, kaons and their sum, integrated over energy and zenith angle. These values correspond to the bracket term in eq. 2. The upper pressure layers carry the largest weights, due to $P_\mu(E_0, \theta, \chi)$ being large at low χ, and thus temperature changes in the upper atmosphere are expected to be of largest influence on the muon rate. The higher frequency of data-taking runs was used to estimate the change of the muon rate during a 12 hour interval, which was used for the systematical uncertainty of the correlation. In order to match the frequency of the atmospheric temperature data, the KM3NeT dataset was re-sampled to periods of 12 hours.

6. Results

The challenge to extract the muon rate variations with time are illustrated in figure 3(top), where both the measured muon rates from data and the predicted muon rate from the run-by-run simulation are presented. Much of the variations in the muon rate can be attributed to the ambient conditions as they are very well reproduced with the constant flux used in the simulation. Qualitatively, the changes in muon rate are well reproduced, in particular at the shorter timescales. There seem to be some longer time-scale variations that are not seen in the simulated data.

The merit of the method introduced, where the measured rate is divided by the predicted rate $R_{\frac{data}{sim}}(t)$, per formula 4 is illustrated in figure 3(bottom). While there are still short time variations, these are much suppressed and a periodic modulation can be seen. The amplitude of this modulation is around 2 to 3 %, while the period seems consistent with a year. The highest rates are in the Northern summer of 2020. A lower peak in 2021 seems in line with an overall decrease in rate over the analysed period.

A correlation plot of the relative change in rate $\Delta R_{\frac{data}{sim}}/\langle R_{\frac{data}{sim}}\rangle$ with the relative change in effective temperature $\Delta T_{eff}/\langle T_{eff}\rangle$ for 12 hour bins is shown in figure 4. The error bars on the points are from figure 2 and 3 and include several sources of uncertainties besides the statistical errors. Included are the errors on the measurement of the temperature for each pressure layer, the uncertainty due to rate variations at time-scales smaller than 12 hours, and a conservative uncertainty on the effective area of 10 %. There is a clear correlation between the effective temperature and the muon rate. Several clusters of correlated points suggest that there are other effects that are not accounted for. For example, the cluster of points at the right below the fit line, are all of the same period in July 2021.

Shown in the figure is a fit of the linear function

$$\Delta R_{\frac{data}{sim}}/\langle R_{\frac{data}{sim}}\rangle = \alpha_{T,\frac{data}{sim}}\Delta T_{eff}/\langle T_{eff}\rangle + \beta, \quad (6)$$

where $\alpha_{T,\frac{data}{sim}}$ and β are free parameters. All uncertainties were taking into account. The value of the slope was $\alpha_{T,\frac{data}{sim}} = 1.005 \pm 0.041$ and with a residual variance $\chi^2/dof = 0.44$. A null-hypothesis fit (of a horizontal line) gave $\beta = 0.041 \pm 0.061$ with $\chi^2/dof = 0.74$.

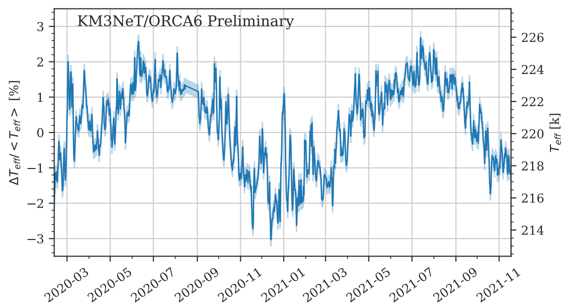

Figure 2: Relative variation (left y-axis) in effective temperature above the ORCA-6 detector. The right y-axis shows the absolute temperature.

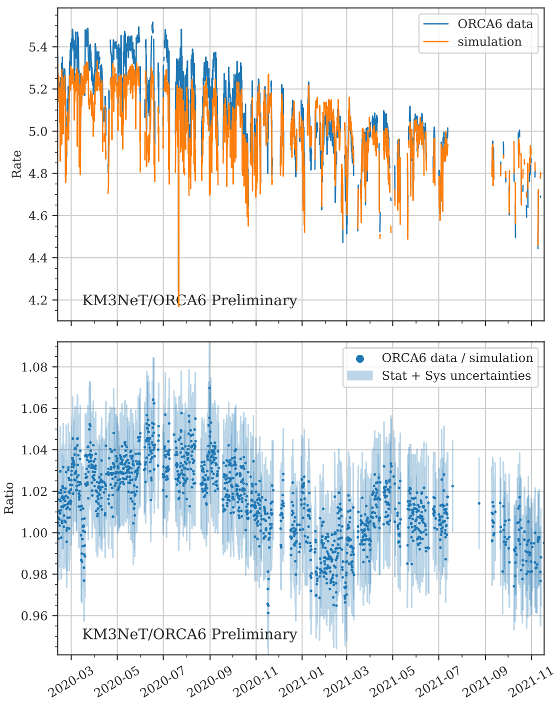

Figure 3: The data and simulated muon rate (top) with their ratio (bottom) for the whole ORCA-6 period. The error-bars (only shown in bottom) include statistical and systematic uncertainties are added in quadrature.

7. Conclusion and Outlook

In this work, a new method to measure the variation in atmospheric muon flux under changing local ambient conditions and efficiency of the KM3NeT detectors has been presented. This was applied to the KM3NeT/ORCA-6 dataset and a correlation of the high energy muon rate with the effective temperature was found. In this first study, simplified, analytic, models have been used for the muon production and propagation, combined with a parametric simulation of the muon flux in the water. Hints towards more complex time-dependent effects on the muon rate require further study, in order to understand whether they originate from the atmosphere or detector

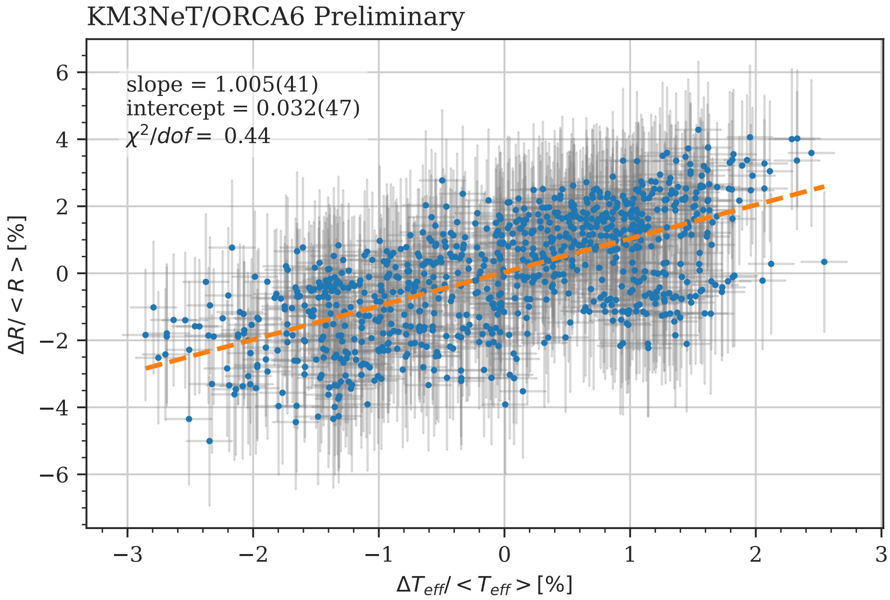

Figure 4: Relative variation in percentage of the effective temperature T_{eff} and data/simulation ratio $R_{\frac{\text{Data}}{\text{Simulation}}}$. The orange dashed line is eq. 6 fitted to the data, using y = slope $\times\, x$ + intercept. The fit takes into account both uncertainties.

and environmental effects that are not corrected for in the simulations. In future studies a more detailed modelling e.g. by the use of full extensive air-shower simulations will be used, together with data from the growing ORCA and ARCA detectors.

References

[1] R. Abbasi et al. "Observation of Seasonal Variations of the Flux of High-Energy Atmospheric Neutrinos with IceCube". In: (Mar. 2023). arXiv: 2303.04682 [astro-ph.HE].

[2] P. Adamson et al. "Observation of Muon Intensity Variations by Season with the MINOS Near Detector". In: *Phys. Rev. D* 90.1 (2014), p. 012010. DOI: 10.1103/PhysRevD.90.012010. arXiv: 1406.7019 [hep-ex].

[3] S. Adrián-Martínez et al. "Deep sea tests of a prototype of the KM3NeT digital optical module". In: *Eur. Phys. J. C* 74.9 (2014), p. 3056. DOI: 10.1140/epjc/s10052-014-3056-3. arXiv: 1405.0839 [astro-ph.IM].

[4] S. Adrián-Martínez et al. "The prototype detection unit of the KM3NeT detector". In: *Eur. Phys. J. C* 76.2 (2016), p. 54. DOI: 10.1140/epjc/s10052-015-3868-9. arXiv: 1510.01561 [astro-ph.IM].

[5] N. Agafonova et al. "Measurement of the cosmic ray muon flux seasonal variation with the OPERA detector". In: *JCAP* (Oct. 2019), p. 003. DOI: 10.1088/1475-7516/2019/10/003.

[6] N. Yu. Agafonova et al. "Characterization of the varying flux of atmospheric muons measured with the Large Volume Detector for 24 years". In: *Phys. Rev. D* 100.6 (2019), p. 062002. DOI: 10.1103/PhysRevD.100.062002. arXiv: 1909.04579 [astro-ph.HE].

[7] AIRS project. *Aqua/AIRS L3 Daily Standard Physical Retrieval (AIRS-only) 1 degree x 1 degree V7.0*. 2019. DOI: 10.5067/UO3Q64CTTS1U. URL: https://disc.gsfc.nasa.gov/datasets/AIRS3STD_7.0/summary.

[8] I. Alekseev et al. "Observation of the temperature and barometric effects on the cosmic muon flux by the DANSS detector". In: *Eur. Phys. J. C* 82.6 (2022), p. 515. DOI: 10.1140/epjc/s10052-022-10471-1. arXiv: 2112.03702 [physics.ins-det].

[9] M. Ambrosio et al. "Seasonal variations in the underground muon intensity as seen by MACRO". In: *Astroparticle Physics* 7.1 (1997), pp. 109–124. ISSN: 0927-6505. DOI: https://doi.org/10.1016/S0927-6505(97)00011-X.

[10] F.P. An et al. "Seasonal variation of the underground cosmic muon flux observed at Daya Bay". In: *JCAP* (Jan. 2018), p. 001. DOI: 10.1088/1475-7516/2018/01/001.

[11] Paul h. Barrett et al. "Interpretation of Cosmic-Ray Measurements Far Underground". In: *Review of Modern Physics* 24.3 (July 1952).

[12] G. Carminati, A. Margiotta, and M. Spurio. "Atmospheric MUons from PArametric formulas: A Fast GEnerator for neutrino telescopes (MUPAGE)". In: *Comput. Phys. Commun.* 179 (2008), pp. 915–923. DOI: 10.1016/j.cpc.2008.07.014. arXiv: 0802.0562 [physics.ins-det].

[13] KM3NeT Collaboration. *KM3NeT Technical Design Report*. Tech. rep.

[14] Thomas K. Gaisser, Ralph Engel, and Elisa Resconi. *Cosmic Rays and Particle Physics*. 2nd ed. Cambridge University Press, 2016. DOI: 10.1017/CBO9781139192194.

[15] E.W. Grashorn et al. "The atmospheric charged kaon/pion ratio using seasonal variation methods". In: *Astroparticle Physics* 33.3 (2010), pp. 140–145. ISSN: 0927-6505. DOI: 10.1016/j.astropartphys.2009.12.006.

[16] Brían Ó Fearraigh. "Tuning parametric models of the atmospheric muon flux in MUPAGE to data from the KM3NeT detector". In: *PoS* ICRC2021 (2021), p. 1176. DOI: 10.22323/1.395.1176.

[17] H. Prihtiadi et al. "Measurement of the cosmic muon annual and diurnal flux variation with the COSINE-100 detector". In: *JCAP* 02 (2021), p. 013. DOI: 10.1088/1475-7516/2021/02/013. arXiv: 2005.13672 [physics.ins-det].

[18] A. Romanov. "Comparison of the atmospheric muon flux measured by the KM3NeT detectors with the CORSIKA simulation using the Global Spline Fit model". In: *PoS* ICRC2023 (2023).

[19] Serap Tilav et al. "Seasonal variation of atmospheric muons in IceCube". In: *PoS* ICRC2019 (2020), p. 894. DOI: 10.22323/1.358.0894.

Full Authors List: The KM3NeT Collaboration

S. Aiello[a], A. Albert[b,bd], S. Alves Garre[c], Z. Aly[d], A. Ambrosone[f,e], F. Ameli[g], M. Andre[h], E. Androutsou[i], M. Anguita[j], L. Aphecetche[k], M. Ardid[l], S. Ardid[l], H. Atmani[m], J. Aublin[n], L. Bailly-Salins[o], Z. Bardačová[q,p], B. Baret[n], A. Bariego-Quintana[c], S. Basegmez du Pree[r], Y. Becherini[n], M. Bendahman[m,n], F. Benfenati[t,s], M. Benhassi[u,e], D.M. Benoit[v], E. Berbee[r], V. Bertin[d], S. Biagi[w], M. Boettcher[x], D. Bonanno[w], J. Boumaaza[m], M. Bouta[y], M. Bouwhuis[r], C. Bozza[z,e], R.M. Bozza[f,e], H.Brânzaş[aa], F. Bretaudeau[k], R. Bruijn[ab,r], J. Brunner[d], R. Bruno[a], E. Buis[ac,r], R. Buompane[u,e], J. Busto[d], B. Caiffi[ad], D. Calvo[c], S. Campion[g,ae], A. Capone[g,ae], F. Carenini[t,s], V. Carretero[c], T. Cartraud[n], P. Castaldi[af,s], V. Cecchini[c], S. Celli[g,ae], L. Cerisy[d], M. Chabab[ag], M. Chadolias[ah], A. Chen[ai], S. Cherubini[aj,w], T. Chiarusi[s], M. Circella[ak], R. Cocimano[w], J.A.B. Coelho[n], A. Coleiro[n], R. Coniglione[w] P. Coyle[d], A. Creusot[n], A. Cruz[al], G. Cuttone[w], R. Dallier[k], Y. Darras[ah], A. De Benedittis[e], B. De Martino[d], V. Decoene[k], R. Del Burgo[e], U.M. Di Cerbo[e], L.S. Di Mauro[w], I. Di Palma[g,ae], A.F. Díaz[j], C. Diaz[j], D. Diego-Tortosa[w], C. Distefano[w], A. Domi[ah], C. Donzaud[n], D. Dornic[d], M. Dörr[am], E. Drakopoulou[i], D. Drouhin[b,bd], R. Dvornický[q], T. Eberl[ah], E. Eckerová[q,p], A. Eddymaoui[m], T. van Eeden[r], M. Eff[n], D. van Eijk[r], I. El Bojaddaini[y], S. El Hedri[n], A. Enzenhöfer[d], G. Ferrara[w], M. D. Filipović[an], F. Filippini[t,s], D. Franciotti[w], L.A. Fusco[z,e], J. Gabriel[ao], S. Gagliardini[g], T. Gal[ah], J. García Méndez[l], A. Garcia Soto[c], C. Gatius Oliver[r], N. Geißelbrecht[ah], H. Ghaddari[y], L. Gialanella[e,u], B.K. Gibson[v], E. Giorgio[w], I. Goos[n], D. Goupilliere[o], S.R. Gozzini[c], R. Gracia[ah], K. Graf[ah], C. Guidi[ap,ad], B. Guillon[o], M. Gutiérrez[aq], H. van Haren[ar], A. Heijboer[r], A. Hekalo[am], L. Hennig[ah], J.J. Hernández-Rey[c], F. Huang[d], W. Idrissi Ibnsalih[e], G. Illuminati[s], C.W. James[al], M. de Jong[as,r], P. de Jong[ab,r], B.J. Jung[r], P. Kalaczyński[at,be], O. Kalekin[ah], U.F. Katz[ah], N.R. Khan Chowdhury[c], A. Khatun[q], G. Kistauri[av,au], C. Kopper[ah], A. Kouchner[aw,n], V. Kulikovskiy[ad], R. Kvatadze[av], M. Labalme[o], R. Lahmann[ah], G. Larosa[w], C. Lastoria[d], A. Lazo[c], S. Le Stum[d], G. Lehaut[o], E. Leonora[a], N. Lessing[c], G. Levi[t,s], M. Lindsey Clark[n], F. Longhitano[a], J. Majumdar[r], L. Malerba[ad], F. Mamedov[p], J. Mańczak[c], A. Manfreda[e], M. Marconi[ap,ad], A. Margiotta[t,s], A. Marinelli[e,f], C. Markou[i], L. Martin[k], J.A. Martínez-Mora[l], F. Marzaioli[u,e], M. Mastrodicasa[ae,g], S. Mastroianni[e], S. Miccichè[w], G. Miele[f,e], P. Migliozzi[e], E. Migneco[w], M.L. Mitsou[e], C.M. Mollo[e], L. Morales-Gallegos[u,e], C. Morley-Wong[al], A. Moussa[y], I. Mozun Mateo[ay,ax], J. M. Mulder[ab], R. Muller[r], M.R. Musone[e,u], M. Musumeci[w], L. Nauta[r], S. Navas[aq], A. Nayerhoda[ak], C.A. Nicolau[g], B. Nkosi[ai], B. Ó Fearraigh[ab,r], V. Oliviero[f,e], A. Orlando[w], E. Oukacha[n], D. Paesani[w], J. Palacios González[c], G. Papalashvili[au], V. Parisi[ap,ad], E.J. Pastor Gomez[c], A. M. Păun[aa], G.E. Păvălaş[aa], S. Peña Martínez[n], M. Perrin-Terrin[d], J. Perronnel[o], V. Pestel[ay], R. Pestes[n], P. Piattelli[w], C. Poirè[z,e], V. Popa[aa], T. Pradier[b], S. Pulvirenti[w], G. Quéméner[o], C. Quiroz[l], U. Rahaman[c], N. Randazzo[a], R. Randriatoamanana[k], S. Razzaque[az], I.C. Rea[e], D. Real[c], S. Reck[ah], G. Riccobene[w], J. Robinson[x], A. Romanov[ap,ad], A. Šaina[c], F. Salesa Greus[c], D.F.E. Samtleben[as,r], A. Sánchez Losa[c,ak], S. Sanfilippo[w], M. Sanguineti[ap,ad], C. Santonastaso[ba,e], D. Santonocito[w], P. Sapienza[w], J. Schnabel[ah], J. Schumann[ah], H. M. Schutte[x], J. Seneca[r], N. Sennan[y], B. Setter[ah], I. Sgura[ak], R. Shanidze[au], Y. Shitov[p], F. Šimkovic[q], A. Simonelli[e], A. Sinopoulou[a], M.V. Smirnov[ah], B. Spisso[e], M. Spurio[t,s], D. Stavropoulos[i], I. Štekl[p], M. Taiuti[ap,ad], Y. Tayalati[m], H. Tedjditi[ad], H. Thiersen[x], I. Tosta e Melo[a,aj], B. Trocmé[n], V. Tsourapis[i], E. Tzamariudaki[i], A. Vacheret[o], V. Valsecchi[w], V. Van Elewyck[aw,n], G. Vannoye[d], G. Vasileiadis[bb], F. Vazquez de Sola[r], C. Verilhac[n], A. Veutro[g,ae], S. Viola[w], D. Vivolo[u,e], J. Wilms[bc], E. de Wolf[ab,r], H. Yepes-Ramirez[l], G. Zarpapis[i], S. Zavatarelli[ad], A. Zegarelli[g,ae], D. Zito[w], J.D. Zornoza[c], J. Zúñiga[c], and N. Zywucka[x].

[a] INFN, Sezione di Catania, Via Santa Sofia 64, Catania, 95123 Italy
[b] Université de Strasbourg, CNRS, IPHC UMR 7178, F-67000 Strasbourg, France
[c] IFIC - Instituto de Física Corpuscular (CSIC - Universitat de València), c/Catedrático José Beltrán, 2, 46980 Paterna, Valencia, Spain
[d] Aix Marseille Univ, CNRS/IN2P3, CPPM, Marseille, France
[e] INFN, Sezione di Napoli, Complesso Universitario di Monte S. Angelo, Via Cintia ed. G, Napoli, 80126 Italy
[f] Università di Napoli "Federico II", Dip. Scienze Fisiche "E. Pancini", Complesso Universitario di Monte S. Angelo, Via Cintia ed. G, Napoli, 80126 Italy
[g] INFN, Sezione di Roma, Piazzale Aldo Moro 2, Roma, 00185 Italy
[h] Universitat Politècnica de Catalunya, Laboratori d'Aplicacions Bioacústiques, Centre Tecnològic de Vilanova i la Geltrú, Avda. Rambla Exposició, s/n, Vilanova i la Geltrú, 08800 Spain
[i] NCSR Demokritos, Institute of Nuclear and Particle Physics, Ag. Paraskevi Attikis, Athens, 15310 Greece
[j] University of Granada, Dept. of Computer Architecture and Technology/CITIC, 18071 Granada, Spain
[k] Subatech, IMT Atlantique, IN2P3-CNRS, Université de Nantes, 4 rue Alfred Kastler - La Chantrerie, Nantes, BP 20722 44307 France
[l] Universitat Politècnica de València, Instituto de Investigación para la Gestión Integrada de las Zonas Costeras, C/ Paranimf, 1, Gandia, 46730 Spain
[m] University Mohammed V in Rabat, Faculty of Sciences, 4 av. Ibn Battouta, B.P. 1014, R.P. 10000 Rabat, Morocco
[n] Université Paris Cité, CNRS, Astroparticule et Cosmologie, F-75013 Paris, France
[o] LPC CAEN, Normandie Univ, ENSICAEN, UNICAEN, CNRS/IN2P3, 6 boulevard Maréchal Juin, Caen, 14050 France
[p] Czech Technical University in Prague, Institute of Experimental and Applied Physics, Husova 240/5, Prague, 110 00 Czech Republic
[q] Comenius University in Bratislava, Department of Nuclear Physics and Biophysics, Mlynska dolina F1, Bratislava, 842 48 Slovak Republic
[r] Nikhef, National Institute for Subatomic Physics, PO Box 41882, Amsterdam, 1009 DB Netherlands
[s] INFN, Sezione di Bologna, v.le C. Berti-Pichat, 6/2, Bologna, 40127 Italy
[t] Università di Bologna, Dipartimento di Fisica e Astronomia, v.le C. Berti-Pichat, 6/2, Bologna, 40127 Italy
[u] Università degli Studi della Campania "Luigi Vanvitelli", Dipartimento di Matematica e Fisica, viale Lincoln 5, Caserta, 81100 Italy
[v] E. A. Milne Centre for Astrophysics, University of Hull, Hull, HU6 7RX, United Kingdom

[w]INFN, Laboratori Nazionali del Sud, Via S. Sofia 62, Catania, 95123 Italy
[x]North-West University, Centre for Space Research, Private Bag X6001, Potchefstroom, 2520 South Africa
[y]University Mohammed I, Faculty of Sciences, BV Mohammed VI, B.P. 717, R.P. 60000 Oujda, Morocco
[z]Università di Salerno e INFN Gruppo Collegato di Salerno, Dipartimento di Fisica, Via Giovanni Paolo II 132, Fisciano, 84084 Italy
[aa]ISS, Atomistilor 409, Măgurele, RO-077125 Romania
[ab]University of Amsterdam, Institute of Physics/IHEF, PO Box 94216, Amsterdam, 1090 GE Netherlands
[ac]TNO, Technical Sciences, PO Box 155, Delft, 2600 AD Netherlands
[ad]INFN, Sezione di Genova, Via Dodecaneso 33, Genova, 16146 Italy
[ae]Università La Sapienza, Dipartimento di Fisica, Piazzale Aldo Moro 2, Roma, 00185 Italy
[af]Università di Bologna, Dipartimento di Ingegneria dell'Energia Elettrica e dell'Informazione "Guglielmo Marconi", Via dell'Università 50, Cesena, 47521 Italia
[ag]Cadi Ayyad University, Physics Department, Faculty of Science Semlalia, Av. My Abdellah, P.O.B. 2390, Marrakech, 40000 Morocco
[ah]Friedrich-Alexander-Universität Erlangen-Nürnberg (FAU), Erlangen Centre for Astroparticle Physics, Nikolaus-Fiebiger-Straße 2, 91058 Erlangen, Germany
[ai]University of the Witwatersrand, School of Physics, Private Bag 3, Johannesburg, Wits 2050 South Africa
[aj]Università di Catania, Dipartimento di Fisica e Astronomia "Ettore Majorana", Via Santa Sofia 64, Catania, 95123 Italy
[ak]INFN, Sezione di Bari, via Orabona, 4, Bari, 70125 Italy
[al]International Centre for Radio Astronomy Research, Curtin University, Bentley, WA 6102, Australia
[am]University Würzburg, Emil-Fischer-Straße 31, Würzburg, 97074 Germany
[an]Western Sydney University, School of Computing, Engineering and Mathematics, Locked Bag 1797, Penrith, NSW 2751 Australia
[ao]IN2P3, LPC, Campus des Cézeaux 24, avenue des Landais BP 80026, Aubière Cedex, 63171 France
[ap]Università di Genova, Via Dodecaneso 33, Genova, 16146 Italy
[aq]University of Granada, Dpto. de Física Teórica y del Cosmos & C.A.F.P.E., 18071 Granada, Spain
[ar]NIOZ (Royal Netherlands Institute for Sea Research), PO Box 59, Den Burg, Texel, 1790 AB, the Netherlands
[as]Leiden University, Leiden Institute of Physics, PO Box 9504, Leiden, 2300 RA Netherlands
[at]National Centre for Nuclear Research, 02-093 Warsaw, Poland
[au]Tbilisi State University, Department of Physics, 3, Chavchavadze Ave., Tbilisi, 0179 Georgia
[av]The University of Georgia, Institute of Physics, Kostava str. 77, Tbilisi, 0171 Georgia
[aw]Institut Universitaire de France, 1 rue Descartes, Paris, 75005 France
[ax]IN2P3, 3, Rue Michel-Ange, Paris 16, 75794 France
[ay]LPC, Campus des Cézeaux 24, avenue des Landais BP 80026, Aubière Cedex, 63171 France
[az]University of Johannesburg, Department Physics, PO Box 524, Auckland Park, 2006 South Africa
[ba]Università degli Studi della Campania "Luigi Vanvitelli", CAPACITY, Laboratorio CIRCE - Dip. Di Matematica e Fisica - Viale Carlo III di Borbone 153, San Nicola La Strada, 81020 Italy
[bb]Laboratoire Univers et Particules de Montpellier, Place Eugène Bataillon - CC 72, Montpellier Cédex 05, 34095 France
[bc]Friedrich-Alexander-Universität Erlangen-Nürnberg (FAU), Remeis Sternwarte, Sternwartstraße 7, 96049 Bamberg, Germany
[bd]Université de Haute Alsace, rue des Frères Lumière, 68093 Mulhouse Cedex, France
[be]AstroCeNT, Nicolaus Copernicus Astronomical Center, Polish Academy of Sciences, Rektorska 4, Warsaw, 00-614 Poland

Acknowledgements

The authors acknowledge the financial support of the funding agencies: Agence Nationale de la Recherche (contract ANR-15-CE31-0020), Centre National de la Recherche Scientifique (CNRS), Commission Européenne (FEDER fund and Marie Curie Program), LabEx UnivEarthS (ANR-10-LABX-0023 and ANR-18-IDEX-0001), Paris Île-de-France Region, France; Shota Rustaveli National Science Foundation of Georgia (SRNSFG, FR-22-13708), Georgia; The General Secretariat of Research and Innovation (GSRI), Greece Istituto Nazionale di Fisica Nucleare (INFN), Ministero dell'Università e della Ricerca (MIUR), PRIN 2017 program (Grant NAT-NET 2017W4HA7S) Italy; Ministry of Higher Education, Scientific Research and Innovation, Morocco, and the Arab Fund for Economic and Social Development, Kuwait; Nederlandse organisatie voor Wetenschappelijk Onderzoek (NWO), the Netherlands; The National Science Centre, Poland (2021/41/N/ST2/01177); The grant "AstroCeNT: Particle Astrophysics Science and Technology Centre", carried out within the International Research Agendas programme of the Foundation for Polish Science financed by the European Union under the European Regional Development Fund; National Authority for Scientific Research (ANCS), Romania; Grants PID2021-124591NB-C41, -C42, -C43 funded by MCIN/AEI/ 10.13039/501100011033 and, as appropriate, by "ERDF A way of making Europe", by the "European Union" or by the "European Union NextGenerationEU/PRTR", Programa de Planes Complementarios I+D+I (refs. ASFAE/2022/023, ASFAE/2022/014), Programa Prometeo (PROMETEO/2020/019) and GenT (refs. CIDEGENT/2018/034, /2019/043, /2020/049. /2021/23) of the Generalitat Valenciana, Junta de Andalucía (ref. SOMM17/6104/UGR, P18-FR-5057), EU: MSC program (ref. 101025085), Programa María Zambrano (Spanish Ministry of Universities, funded by the European Union, NextGenerationEU), Spain; The European Union's Horizon 2020 Research and Innovation Programme (ChETEC-INFRA - Project no. 101008324).